Phys Chem Minerals (1989) 16:790–798

PHYSICS AND CHEMISTRY OF MINERALS

X-Ray Diffraction Study of the Orientational Order/Disorder Transition in $NaNO_3$: Evidence for Order Parameter Coupling

Wolfgang Wilhelm Schmahl and Ekhard Salje
Department of Earth Sciences, University of Cambridge, Downing Street, Cambridge CB2 3EQ, England

Abstract. The orientational ordering transition $R\bar{3}m - R\bar{3}c$ in $NaNO_3$ near 552 K has been investigated using x-ray diffraction techniques. $NaNO_3$ is a model system for $CaCO_3$ and other minerals with orientational disorder of triangular molecules in a simple NaCl-type matrix. The temperature evolution of the integrated intensities of the superlattice reflection $\bar{1}23$ and the fundamental reflection *110* are discussed in terms of Landau theory of two coupled order parameters. It is shown that the known phenomenological critical exponent (Poon and Salje 1988) and the anomalous thermal expansion at $T > T_{tr}$ (Reeder et al. 1988) can be understood as the result of a Z point instability which mainly describes the NO_3^- disorder, and a second order parameter linked with the spontaneous strain of this phase transition.

1. Introduction

The phase transition in $NaNO_3$ near 552 K has attracted much attention during the last two decades because it is generally considered as a prototype of a λ-transition with a large excess specific heat anomaly (Reinsborough and Wetmore 1957). This phase transition is also structurally and thermodynamically closely related to the $R\bar{3}m - R\bar{3}c$ phase transition in Calcite (Salje and Viswanathan 1976, Dove and Powell 1989, Redfern et al. 1989) so that $NaNO_3$ is a model compound for a large group of structures where small triangular molecules order in a NaCl-like matrix. The first structural interpretation of this phase transition is due to Kracek (1931) and Kracek et al. (1931) who determined the correct space groups of the high temperature phase (i.e. $R\bar{3}m$) and of the low temperature phase (i.e. $R\bar{3}c$) and noted that the reflections *hkl* with *l* odd (with respect to the hexagonal setting of the low temperature phase) are superlattice reflections and have zero intensity in the disordered phase. Further crystallographic work by Strømme (1969), Paul and Pryor (1972), Terauchi and Yamada (1972) and Lefebvre et al. (1984) lead to a more detailed model of the molecular disordering process, the results of other physical experiments such as NMR (D'Alessio and Scott 1971), Raman Spectroscopy (e.g. Shen et al. 1975; Neumann and Vogt 1978; Yasaka et al. 1985), infrared spectroscopy (e.g. Brehat and Wyncke 1985) and inelastic neutron scattering (e.g. Lefebvre et al. 1980) stressed the relationship between the structural aspects of the phase transition and the dynamics of the $NaNO_3$ lattice. Recent investigations in our laboratory showed the importance of elastic interactions and the developement of spontaneous strain both in $NaNO_3$ and $CaCO_3$ (Poon and Salje 1988; Reeder et al. 1988; Dove and Powell 1989; Redfern et al. 1989). The studies revealed the close correlation between the strong expansion of the unit cell along the crystallographic **c**-axis $[001]_{hex}$ (and the weak variations in the **a**, **b** plane) and the thermodynamic properties of the phase transition. Molecular dynamics calculations by Lynden-Bell et al. (1989) also stress the importance of the coupling between the rotational and translational degrees of freedom of the NO_3^- molecules and the change of the size of the crystallographic unit cell. Both effects and their coupling contribute significantly to the total excess Gibbs free energy of this phase transition.

In this paper we report the results of x-ray diffraction experiments between room temperature and ca. 570 K (the bulk melting point of $NaNO_3$ is 583 K) in which the temperature dependence of the intensities of selected reflections related to the phase transition were studied in detail. We will show that the structural phase transition is driven by two mechanisms which combine to break the $R\bar{3}m$ symmetry. The results will be quantified within the framework of Landau theory.

2. Experimental

$NaNO_3$ single crystals of high quality grown from aqueous solutions were kindly provided by Prof. P.J. Herley of the State University of New York at Stony Brook. These samples were also used for other investigations of $NaNO_3$ in our laboratory (Poon and Salje 1988; Reeder et al. 1988; Wruck 1987).

A cleaved regular rhombohedron with 0.5 mm edge-to-edge diameter was mounted with ceramic cement (SiO_2 based) on a silica glass fibre cemented into a stainless steel rod. The mount was preheated for 2 days at 450 K and then fitted on the stainless steel goniometer head of a Philips PW1100 4-circle diffractometer, equipped with a Mo x-ray fine focus tube and a graphite monochromator. A 0.8 mm beam collimator was used along with horizontal and vertical detector apertures of 2° and 1.5°, respectively. A furnace rotating with the χ circle was centered around the crystal in the Eulerian cradle. The heater design followed Brown et al. (1973), with a cylindrical pyrophyllite body (2 cm ∅) containing the heating elements and conical diffraction apertures of 30°, covered with capton windows. A Eurotherm

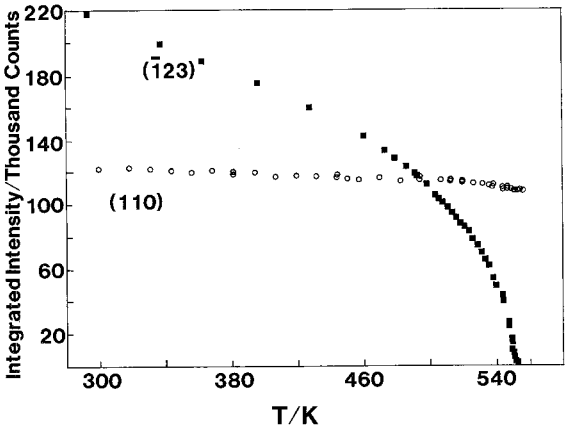

Fig. 1. Temperature evolution of the integrated intensity of the fundamental reflection *110* and of the superlattice reflection $\bar{1}23$

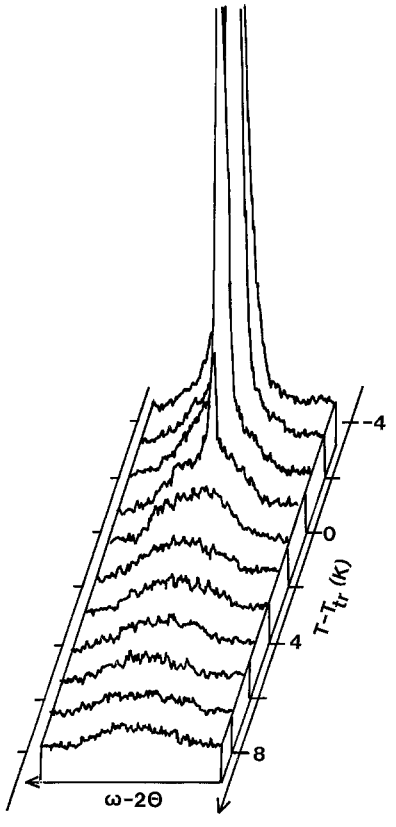

Fig. 2. Profiles of Bragg – and diffuse scattering around $\bar{1}23$ near T_{tr}

controller was used which allowed a relative temperature stability of ± 0.25 K as measured using a chromel-alumel thermocouple set 0.5 mm from the surface of the crystal. Diffraction intensities were recorded using continuous $\omega - 2\theta$ scans covering 2° ω with scan speeds between 0.001° and 0.02° ω/s. The background scattering was measured for half the scan time on either side of the scan. The total background was interpolated and subtracted from the measured total signal.

For accurate determination of the temperature dependence of a single diffraction intensity, the Φ and χ angular settings were kept centred on this reflection during the entire measurement at all temperatures. All measurements were repeated several times and reproducibility within 1% was

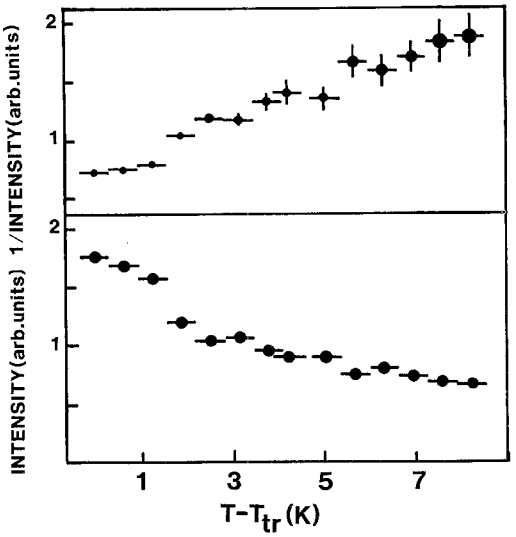

Fig. 3. Temperature dependence of integrated diffuse intensity at $\bar{1}23$ above T_{tr}

found only after annealing the cement for 2 days at 550 K and five complete temperature runs between room temperature and 560 K, which took two more days. The final experiments were then repeated at least 3 times for each reflection over the full temperature range. The absolute temperature calibration (based on in situ observation of first order structural transformations and melting of various materials, and the extrapolated T_c of the power law behaviour of the long range order parameter, see below, known from DSC measurements of the same material, Wruck 1987) is believed to be correct within 0.5 K near T_{tr} and ca. 2 K elsewhere.

3. Results

The temperature evolution of the integrated intensities of the superlattice reflection $\bar{1}23$ and the fundamental reflection *110* are shown in Fig. 1. These reflections were chosen for the experiments because they have similar $\sin\theta/\lambda$ values and hence possess similar Debye-Waller factors. The effect of the Debye-Waller factor is seen in Fig. 1 for the *110* reflection, whereas the $\bar{1}23$ reflection shows the strong temperature dependence of a critical reflection which is fully extinct in the high temperature phase. At temperatures close to the phase transition point, strong diffuse scattering occurs at and near to the position of the $\bar{1}23$ reflection (Fig. 2). The Bragg intensity vanished for temperatures above T_{tr} ≈ 552.3 K (according to our temperature calibration). The temperature dependence of the integrated diffuse scattering intensity above T_{tr} is shown in Fig. 3.

4. Discussion

4.1. Orientational Order and Critical Scattering

In the ideal $R\bar{3}c$ structure the planar NO_3^- molecules are stacked in layers perpendicular to the hexagonal c axis such that the molecules in the same *(001)* layer have identical orientation while the molecules in adjacent layers are rotated by 180° with respect to each other (Fig. 4). (Due to the molecular symmetry the 180° rotation is equivalent to a 60° rotation and to the inversion operation actually relating the molecular positions in adjacent layers in this space

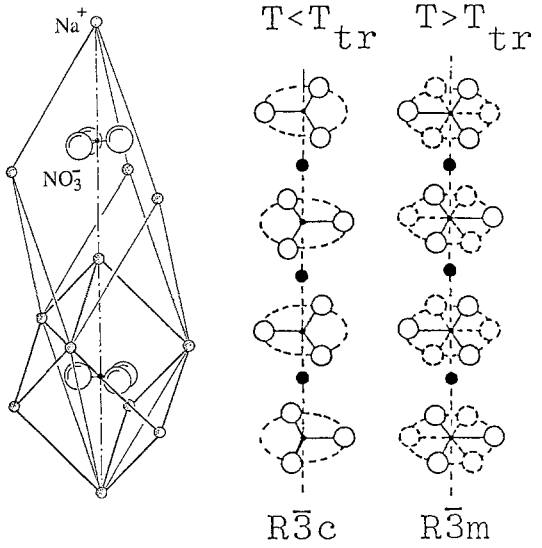

Fig. 4. Sketch of the structure and primitive rhombohedral unit cells of $NaNO_3$ below and above the phase transition temperature

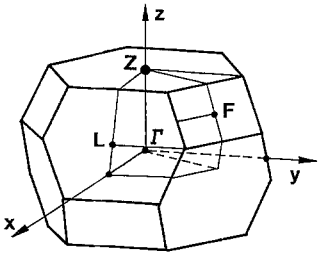

Fig. 5. Schematic view of the Brillouin zone of the disordered ($R\bar{3}m$) phase of $NaNO_3$. The critical long range correlation occurs at the point $\mathbf{Z}=\frac{3}{2}c^*(R\bar{3}m)$

group). With increasing temperature, the orientational correlation decreases continuously, and above the transition temperature near 552 K each molecule is found in both states $\pm\pi$ with equal probability (as a space average). The symmetry of this disordered structure is $R\bar{3}m$ with mirror planes perpendicular to the directions of the N–O bonds and $c_{hex}(R\bar{3}m)=\frac{1}{2}c_{hex}(R\bar{3}c)$.

Without reference to the specific nature of the orientational correlation functions involved (which include librational displacements from the two 'equilibrium' orientational states, Paul and Pryor 1972; Lefebvre et al. 1984), the order parameter system can be defined by a (electron) density correlation function. Let $\varphi_0(\mathbf{x})$ be the average density of the $R\bar{3}m$ structure at a temperature $T \gg T_{tr}$. The local instantaneous density is

$$\varphi(\mathbf{x})=\varphi_0(\mathbf{x})+\Delta\varphi(\mathbf{x}) \tag{4.1.1}$$

where $\Delta\varphi(\mathbf{x})$ is dominated by the orientational disorder. Any orientational correlations with non-vanishing mean square amplitude

$$\langle Q(\mathbf{q})\,Q^*(\mathbf{q})\rangle=\int\int\Delta\varphi(\mathbf{x})\,\Delta\varphi(\mathbf{x}+\mathbf{r})\exp(-i\mathbf{q}\mathbf{r})\,dv_{\mathbf{x}}\,dv_{\mathbf{r}} \tag{4.1.2}$$

give rise to x-ray scattering with intensity

$$I(\mathbf{H}+\mathbf{q})=\int\int(\varphi_0(\mathbf{x})+\Delta\varphi(\mathbf{x}))\,(\varphi_0(\mathbf{x}+\mathbf{r})+\Delta\varphi(\mathbf{x}+\mathbf{r}))\cdot\exp(-i(\mathbf{H}+\mathbf{q})\,\mathbf{r})\,dv_{\mathbf{x}}\,dv_{\mathbf{r}} \tag{4.1.3}$$

$$=I_0(\mathbf{H})\,\delta(\mathbf{q},\mathbf{0})+|F_1(\mathbf{H}+\mathbf{q})|^2\,\langle Q(\mathbf{q})\,Q^*(\mathbf{q})\rangle \tag{4.1.4}$$

where $I_0(\mathbf{H})$ is the Bragg intensity due to $\varphi_0(\mathbf{x})$ at the reciprocal lattice vector $\mathbf{H}$ of the disordered structure and

$$F_1(\mathbf{H}+\mathbf{q})=\int\Delta\varphi_1(\mathbf{x})\exp(-i(\mathbf{H}+\mathbf{q})\,\mathbf{x})\,dv_{\mathbf{x}} \tag{4.1.5}$$

is the structure factor for a density modulation with unit amplitude $Q(\mathbf{q})$. The critical long range correlation leading from the disordered $R\bar{3}m$ to the ordered $R\bar{3}c$ structure occurs at the point $\mathbf{q}=\mathbf{Z}=\frac{3}{2}c^*(R\bar{3}m)$ on the surface of the Brillouin zone (Fig. 5) of the disordered phase. The long range order parameter $Q(\mathbf{Z})$ breaking the macroscopic symmetry is thus given by

$$\langle\mathbf{Q}(\mathbf{q}=\mathbf{Z})\rangle=\int\Delta\varphi(\mathbf{x})\exp(-i\mathbf{q}\mathbf{x})\,dv_{\mathbf{x}} \tag{4.1.6}$$

and leads to the appearance of superlattice Bragg reflections for $T<T_{tr}$ at positions $\mathbf{H}+\mathbf{Z}=hkl$, $l=2n+1$ between the fundamental reflections $\mathbf{H}$, with integer Miller indices hkl referring to the hexagonal setting of the ordered ($R\bar{3}c$) phase[1]. The Bragg intensity of the superlattice reflections follows the square of the order parameter according to

$$I(\mathbf{H}+\mathbf{Z})=|F_1(\mathbf{H}+\mathbf{Z})|^2\,\langle Q(\mathbf{Z})\rangle^2 \tag{4.1.7}$$

and is superimposed on the diffuse scattering as given by (4.1.4). The diffuse intensity which has been observed at temperatures close to and above T_{tr} at wavevectors $\mathbf{Z}+\mathbf{k}$, $\mathbf{k}\to\mathbf{0}$, is thus due to long-wavelength modulations of the $\mathbf{Z}$-point ordering pattern, which most probably result from domain boundaries between ordered clusters. As the ordering process is dominated by correlations at the Brillouin zone boundary, the fundamental reflections are only affected by a Debye-Waller like effect (Paul and Pryor 1972; Lefebvre et al. 1984) which is small for low-order reflections.

4.2. Thermodynamic Modeling

Extending the previous interpretations of order parameter behaviour in $NaNO_3$ which were based on phenomenologic power laws for the order parameter (Poon and Salje 1988; Reeder et al. 1988), we shall attempt a more quantitative understanding of the $NaNO_3$ system within the framework of Landau theory. In a first step, the system is discussed in terms of a single order parameter, i.e. the $\mathbf{Z}$-point long range order parameter Q. It will be shown that this single ordering process is not sufficient to explain our experimental results. Thus, in a second step, we will couple this order parameter Q with a second order parameter P which is relevant at temperatures close to T_{tr}. Only this coupling leads to an appropriate description of our experimental data.

4.2.a. The Z-Point Instability. The symmetry breaking process at the $\mathbf{Z}$-point, which characterizes the $R\bar{3}c$ phase, belongs to the one-dimensional irreducible representation $Z_2(A_{1u})$ (Petzelt and Dvorak 1976).

The magnitude of the long range correlation can thus be described by a single-component order parameter Q, and the corresponding Landau expression for the free energy is

$$G=G_0+\tfrac{1}{2}a(T-T_c)\,Q^2+\tfrac{1}{4}b'Q^4+\tfrac{1}{6}cQ^6+de_3\,Q^2+fe_3^2 \tag{4.2.1}$$

where e_3 is the spontaneous strain along c_{hex}.

[1] The appropriate transformation between the standard hexagonal settings of both lattices is $(hkl)_{R\bar{3}m}=(\bar{h}k2l)_{R\bar{3}c}$ and thus the superlattice reflections have odd indices l with respect to the ordered $R\bar{3}c$ phase. We use the $R\bar{3}c$ setting throughout this paper

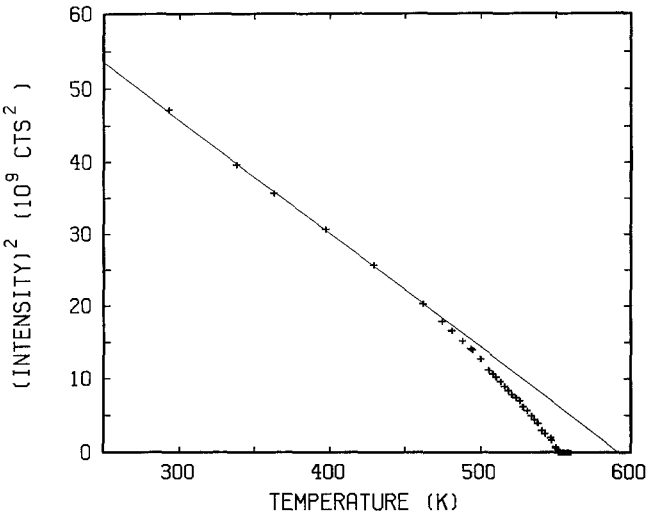

Fig. 6. Square of measured superlattice intensity (corresponding to Q^4) vs. temperature. The solid line represents ideally 'tricritical' ($\beta = 1/4$) behaviour for $T < 460$ K

The well known solutions for equilibrium are (using $b = (b' - d^2/f)$)

$$e_3 = (-d^2/f)\, Q^2 \tag{4.2.2}$$

and

$$Q^2 = \frac{1}{2c}\left(-b + [b^2 - 4a(T - T_c)\, c]^{1/2}\right) \tag{4.2.3}$$

corresponding to a first order transition for $b < 0$ and a continuous transition for $b > 0$.

However, a simple power law behaviour

$$Q \sim Q_0 |T - T_c|^{\beta} \tag{4.2.4}$$

with an effective exponent β and an effective T_c in a limited temperature range may be sufficient to approximate experimental results. The power law behaviour is exact for $b = 0$, $c > 0$ ($\beta = \frac{1}{4}$, Gaussian fix point), the Landau limit with $b > 0$, $c = 0$ is $\beta = \frac{1}{2}$.

The plot of Q^4 versus T in Fig. 6 shows that below ca. 460 K the thermal behaviour can be described by an effectively 'tricritical' behaviour ($b = 0$) with $\beta = \frac{1}{4}$ and $T_c = 592.5 \pm 2$ K. At ca. 460 K a crossover occurs to a region with an effective critical exponent $\beta = 0.22(1)$ and $T_c = 552.4$ K (Schmahl 1988). Starting from (4.2.1), effective exponents $\beta < \frac{1}{4}$ are only possible for transitions with a small first order step ($b < 0$). As shown in Fig. 7a (curve I) the data in the range 460 K–552 K can be fitted with (4.2.3) obtaining a negative value for b and thus a small discontinuity at 551.5 K. However, a discontinuity has not been found experimentally. These results on effective scaling behaviour and a crossover between two thermal regimes are identical to those obtained by measurements of excess birefringence (Poon and Salje 1988), spontaneous strain (Reeder et al. 1988) and excess heat capacity and excess entropy (Wruck 1987).

Figure 7a (curve II) shows the unsatisfactory result obtained by a fit of (4.2.3) over the whole investigated temperature range. This result indicates that the crossover behaviour near 460 K can not be explained as due to two different power law approximations to (4.2.3) and that two different

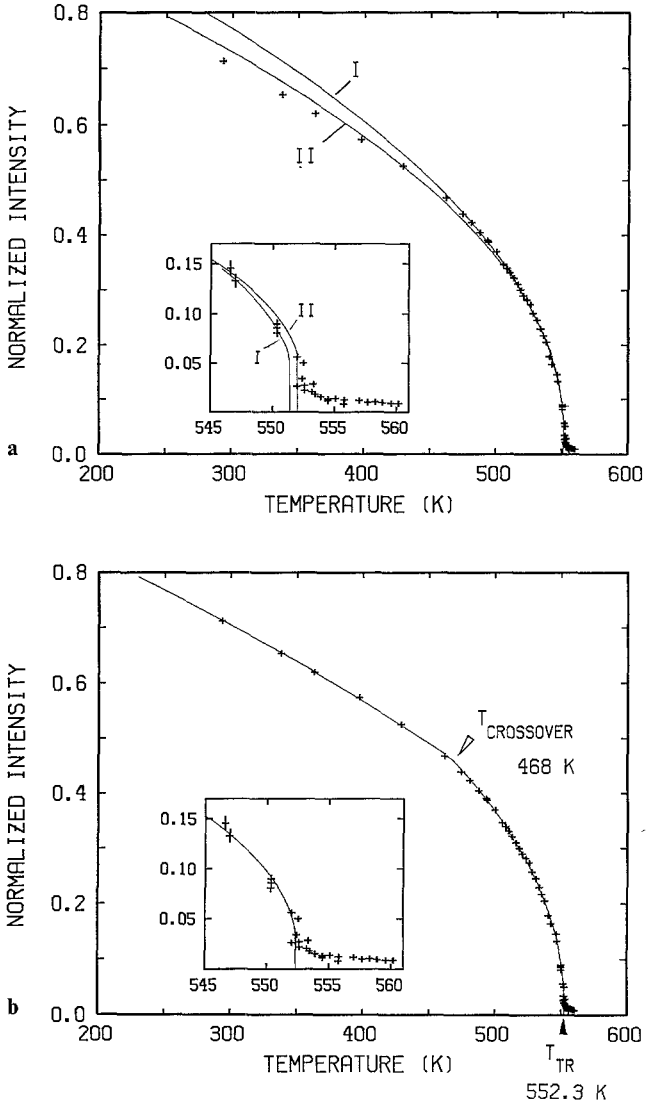

Fig. 7. a Thermodynamic modeling of the observed superlattice intensity assuming a classical first order transition: curve I was obtained by a fit to the data above 460 K only, curve II is the result of a fit over the whole temperature range. **b** Thermodynamic modeling of the observed superlattice intensity using the order parameter coupling model. The two curves corresponding to the parameter sets in Table 1 are indistinguishable on the scale of the diagram

sets of effective single order parameter Landau polynomials are necessary to describe the experimental data.

A weak temperature dependence of other Landau coefficients does not lead to more satisfactory results because all these models show a second systematic deficiency: all measurements on $NaNO_3$ and $CaCO_3$ (Poon and Salje 1988; Reeder et al. 1988; Wruck 1987; Dove and Powell 1989; D'Alessio and Scott 1971; this study) have revealed a pronounced tail of excess property (such as spontaneous strain or excess entropy) persisting above T_{tr} well up to the melting point. This tail (which has been attributed to short range precursor order) is decreasing with increasing temperature and requires a second parameter (or several parameters) coupling to strain etc. and showing a temperature dependence above T_{tr}. For the single order parameter model, both spontaneous strain and excess entropy are de-

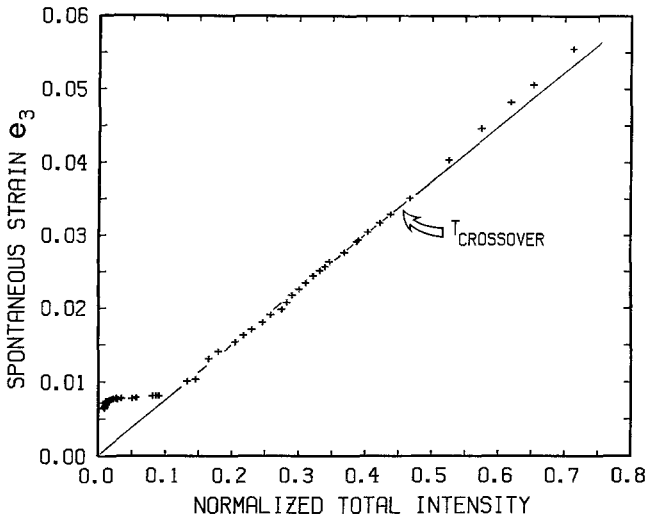

Fig. 8. Spontaneous strain ('intermediate model' of Reeder et al. 1988) vs. total intensity at $\bar{1}23$, i.e. integrated Bragg and diffuse intensity. Note the large excess strain for low values of **Z**-point order

termined by the square of the long range order parameter Q, and thus both quantities must be strictly zero above the transition temperature. The observation of strong diffuse scattering around the **Z**-point suggests that these spatial fluctuations are responsible for the excess strain above T_{tr}. The appropriate Landau-Ginzburg extension of the single order parameter model can easily be written down as

$$G = G_0 + \Sigma_{\mathbf{qq'}} a_{\mathbf{qq}} \langle Q_{\mathbf{q}} Q_{\mathbf{q'}} \rangle (T - T_q) + e_3 d_{\mathbf{qq'}} \langle Q_{\mathbf{q}} Q_{\mathbf{q'}} \rangle + \Sigma_{\mathbf{qq'q''q'''}} b_{\mathbf{qq'q''q'''}} \langle Q_{\mathbf{q}} Q_{\mathbf{q'}} Q_{\mathbf{q''}} Q_{\mathbf{q'''}} \rangle + \ldots \quad (4.2.5)$$

(Bruce and Cowley 1981) where the summations are taken over all fluctuation amplitudes at wave vectors **q**.

The following observations, however, are in variance with the classical Landau-Ginzburg expansion of a single order parameter approach for $NaNO_3$:

i) assuming that the strain coupling constant $d_{\mathbf{qq}}$ varies only slowly with wave vector in the vicinity of **Z**, with the contraction of the c_{hex} lattice parameter increasing with increasing correlation length of the ordered clusters, the diffuse intensity compared to the Bragg intensity should have at least the same magnitude as the strain tail compared to the strain below T_{tr}. Inspection of Fig. 8 shows that the magnitude of the **Z**-point fluctuations appears to be too small to account for the tail of spontaneous strain or excess entropy.

ii) The interpretation of the observed phenomenological exponents as genuine critical exponents faces another problem: strictly the critical exponents are valid only in the Ginzburg interval where critical fluctuations, rather than the long range order, dominate the thermodynamics of the critical behaviour. Numerous investigations of structural phase transitions in minerals and related oxide systems indicate that the Ginzburg interval is generally quite small, in particular in the presence of the long range interactions characteristic for these systems (Bruce and Cowley 1981; Salje 1988). In a recent paper Ginzburg et al. (1987) estimated the size of the interval from the expected interaction length for structural ordering as generally less than 1 K. This is in marked contrast to the ca. 300 K which would have to be assumed for $NaNO_3$. As discussed by Bruce and Cowley (1981), logarithmic corrections have to be applied to tricritical behaviour within the Ginzburg interval according to

$$Q \sim (t)^{\frac{1}{4}} |\log|t||^{\frac{1}{4}}, \quad t = T - T_c/T_c \quad (4.2.6)$$

For $t \to 1$, $|\log|t||^{\frac{1}{4}} \to 0$ and thus this model failed to give an appropriate correction over the large temperature interval in question. With long range interactions present, the system should behave according to classical Landau theory outside the Ginzburg interval. Here it is important to note that Dove and Powell (1989) did not observe any deviation from tricritical Landau behaviour in the isotypic system $CaCO_3$ (Calcite), although a strain-tail similar to that in $NaNO_3$ was observed.

In summary we find that a quantitative description of our experimental results is not possible using a single order parameter Landau theory including classical critical fluctuations.

4.2.b. Order Parameter Coupling. The shortcomings of the single order parameter model strongly suggest that the order/disorder transition is controlled by more than one type of anharmonic process. However, no direct observation of a second ordering or fluctuation process operating in $NaNO_3$ at the relevant temperature and pressure conditions has been reported so far. In view of the missing detailed information about different types of spacial fluctuations and parameters controlling their temperature dependence, we simply assume that the excess free energy can be expanded as a function of the long range order parameter Q characterizing the $R\bar{3}c$ order as in (4.2.1), and the effective macroscopic root mean square amplitude P of a second anharmonic cooperative structural process, dominating above T_{tr}:

$$G = G_0 + \tfrac{1}{2} a_Q (T - T_Q) Q^2 + \tfrac{1}{4} b'_Q Q^4 + \tfrac{1}{6} c_Q Q^6 + d_Q e_3 Q^2 + \tfrac{1}{2} a_P (T - T_P) P^2 + \tfrac{1}{4} b'_P P^4 + d_P e_3 P^2 + \lambda' Q^2 P^2 + f e_3^2 \quad (4.2.7)$$

As P does not seem to lead to a crystallographic long range order in the strict sense in $NaNO_3$, it may represent fluctuations in competing ordering schemes at wave vectors different from **Z** and can be closely linked to local cooperative structural relaxations occuring at the interfaces between ordered $R\bar{3}c$ clusters. We consider biquadratic coupling between P and Q, while terms explicitely describing spacial fluctuations are neglected. No terms higher than P^4 are considered because the temperature interval where experimental data were obtained is limited to $T \ll T_P$. This model of two biquadratically coupled order parameters has already been discussed by Gufan and Larin (1980) and Salje and Devarajan (1986).

The condition $\partial e/\partial Q = 0 = \partial e/\partial P$ for elastic equilibrium leads to a renormalization of the quartic terms and the coupling parameter λ'

$$b_Q = b'_Q - d_Q^2/f \quad (4.2.8)$$

$$b_P = b'_P - d_P^2/f \quad (4.2.9)$$

$$\lambda = \lambda' - d_P d_Q/2f \quad (4.2.10)$$

and four different phases (or thermal regimes) corresponding to solutions for equilibrium (e.g. $\partial G/\partial Q = 0$, $\partial G/\partial P = 0$ etc.) exist (we are using the nomenclature of Salje and Devarajan (1986) for the indication of the different phases):

Table 1. Free energy coefficients for two solutions obtained by least squares fits to the superlattice intensities. Parameters given without estimated standard deviations were only varied while remaining parameters were fixed. The free energy scale was defined by $c_Q=1$ and b_P was calculated by normalization of P (see text). The transition temperatures given below were calculated from the parameter sets

	I	II
a_Q	0.00246 (9)	0.0027 (1)
T_Q(K)	651 (1)	665 (2)
b_Q	0.52 (4)	0.71 (4)
a_P	0.000127	0.000360
T_P(K)	1750	1200
λ	0.177 (4)	0.286 (5)
$T_{\text{crossover}}$(K)	468.7	467.9
T_{tr}(K)	552.3	552.3
Q_0^2	0.036	0.036
R_I	$0.144*10^{-3}$	$0.145*10^{-3}$

Q_0^2 is the value of Q^2 at the transition temperature T_{tr}

$R_I=\Sigma(I_{\text{observed}}-I_{\text{calculated}})^2/\Sigma(I^2_{\text{observed}})$

0: $Q=0, \quad P=0$ (4.2.11)

I: $P=0,$

$$Q^2=\frac{1}{2c_Q}(-b_Q+[b_Q^2-4a_Q(T-T_Q)c_Q]^{\frac{1}{2}}) \quad (4.2.12)$$

II: $Q=0, \quad P^2=-(a_P/b)(T-T_P)$ (4.2.13)

III: $Q\neq 0, \quad P\neq 0$ with

$$Q^2=S_Q(B_Q+[B_Q^2+A_Q(T-T_Q^{\text{III}})]^{\frac{1}{2}}) \quad (4.2.14)$$

where

$$S_Q=(b_P c_Q)^{-1} \quad (4.2.15)$$

$$A_Q=b_P c_Q(2\lambda a_P-a_Q b_P) \quad (4.2.16)$$

$$B_Q=2\lambda^2-\tfrac{1}{2}b_Q b_P \quad (4.2.17)$$

$$T_Q^{\text{III}}=b_P c_Q(a_Q T_Q b_P-2\lambda a_P T_P)/A_Q \quad (4.2.18)$$

and

$$P^2=S_P(B_P-a_P(T-T_P)c_Q b_P \pm[B_P^2+A_P(T-T_P^{\text{III}})]^{\frac{1}{2}}) \quad (4.2.19)$$

with

$$S_P=(b_P^2 c_Q)^{-1} \quad (4.2.20)$$

$$A_P=\lambda^2 b_P c_Q(8\lambda a_P-a_Q b_P) \quad (4.2.21)$$

$$B_P=\lambda b_Q b_P-4\lambda^3 \quad (4.2.22)$$

$$T_P^{\text{III}}=\lambda^2 b_P c_Q(8\lambda a_P T_P-a_Q T_Q b_P)/A_P \quad (4.2.23)$$

(Note that the functional form (4.2.14) for Q^2 vs. temperature is similar to that of equation (4.2.3) for the case of a transition involving only one order parameter.)

This approach offers at least a qualitative understanding of the $NaNO_3$ system and a good approximation to the thermodynamic behaviour. For $NaNO_3$ the thermal regimes 0, I, II, III can be interpreted in the following way:

I: the $R\bar{3}c$ phase of $NaNO_3$ below 460 K, i.e. the 'tricritical' region of Poon and Salje (1988), Reeder et al. (1988);

II: the $R\bar{3}m$ phase above 552 K, where the long range parameter Q is zero, while the amplitude P is responsible for the excess strain and excess entropy observed above

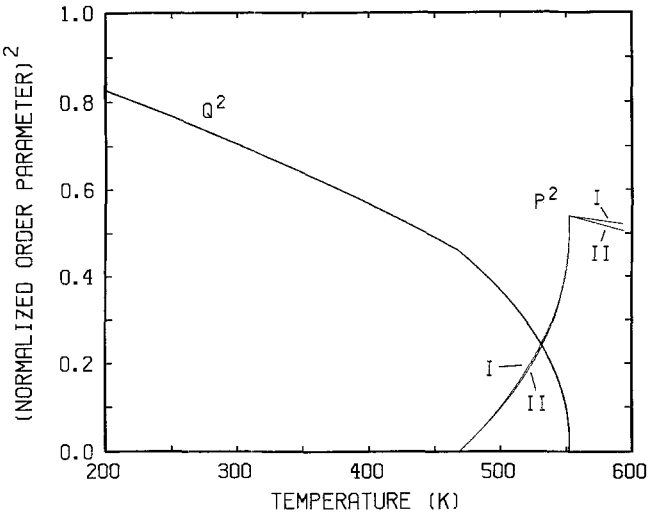

Fig. 9. Comparison of the temperature evolution of the squares of the long range order parameter Q and the coupled order parameter P. Curves I and II represent solutions for the parameter sets I and II of Table 1, the curves for Q^2 are indistinguishable on the scale of the diagram. For better comparison, the values of P^2 have been renormalized to give identical values at T_{tr} for both parameter sets

T_{tr}, which are modelled as linearly dependent on temperature. This is the simplest possible model approximating the behaviour above T_{tr};

III: the region between ca. 460 K and $T_{\text{tr}}=552$ K (the regime previously ascribed to critical fluctuations) where both mechanisms Q and P are thermodynamically relevant.

The phase 0 is irrelevant in this context, as P is not considered to represent a structural distortion leading itself to a phase transition below the melting point at 583 K: the linear term $a_P(T-T_P)$ is merely used to approximate the temperature dependence of the coefficient of P^2 in the temperature range under consideration. The required phase sequence is valid for $T_P>T_Q$, $\lambda>0$. The positive coupling constant λ describes a mutually exclusive nature of the two order parameters or amplitudes: the strongly increasing long range order Q suppresses the amplitude P (possibly a competing ordering scheme) until P completely vanishes at the transition (crossover) III→I.

For numerical calculations we took an extrapolated value of the intensity at O K (according to the solid line in Fig. 6) as scale factor between Q^2 and intensity. The free energy was measured in units of c_Q. As the thermodynamic process characterized by P is only indirectly represented in the superlattice intensity data, the parameters a_P and T_P are not well constrained (b_P was arbitrarily fixed by the normalization $P^2(\text{II, O K})=1=b_P T_P/a_P$). Only four of the free parameters a_Q, b_Q, T_Q, a_P, T_P and λ could be varied simultaneously in least-squares procedures. After each least squares cycle the phase diagram was recalculated on the basis of the current parameter values, and in particular no constraints on the temperatures of the crossover, the main phase transition or the sign of λ were imposed. A 'tricritical' model for phase I (b_Q constrained to 0) resulted in generally unsatisfactory fits including relatively large first order discontinuities for the transition III—II. Thus we varied the parameter b_Q along with the other coefficients until significantly better results as shown in Fig. 7b were achieved. Two parameter sets giving excellent agreement with the

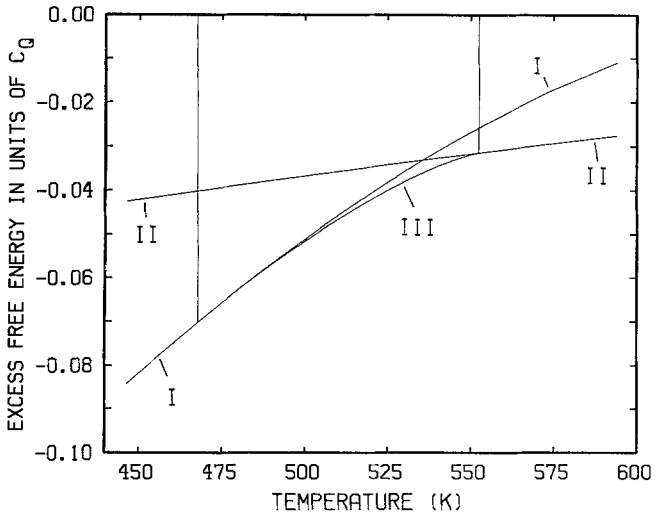

Fig. 10. Excess free energy of the three phases discussed: phase I (long range order at the Z-point only: $P=0, Q\neq 0$), II (no long range order: $Q=0, P\neq 0$) and III (long range order and competing order: $P\neq 0, Q\neq 0$). The vertical lines at 568 K and 552. 3 K indicate the limits of stability for phase III

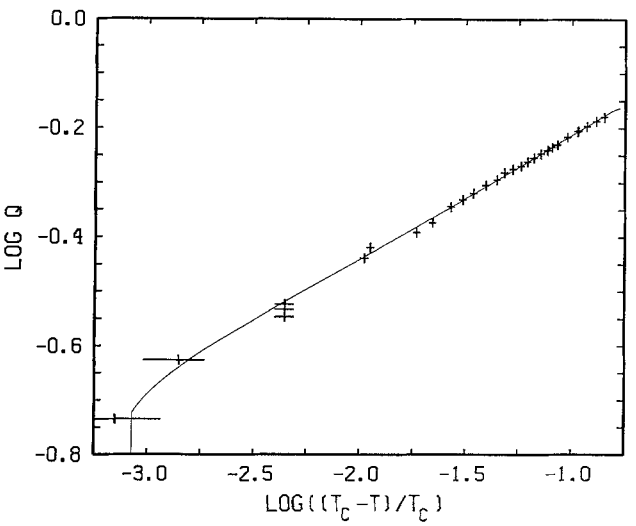

Fig. 11. Plot of $\log[(T-T_c)/T_c]$ vs $(\log[I(\bar{1}23)]/2$ assuming a phenomenological effective T_c of 552.8 K. The solid line represents the data as calculated from model II of Table 1, it is linear in the relevant temperature region with $\beta(\text{eff})=0.227$

data (Fig. 7b, both theoretical curves are identical within the resolution of the plot) are given in Table 1. (The agreement between the nominal transition temperatures as calculated from the free energy model, 552.3 K, and the observed nominal 552.3 K above which the Bragg intensity vanished, Fig. 2, must be regarded as coincidence, given the experimental temperature resulution of ca. ± 0.25 K.) It can be seen by inspection of Fig. 7b and Fig. 9 and by comparing the two parameter sets given in Table 1 that the details of the thermodynamic process characterized by P are hardly relevant to model the behaviour of the observed order parameter Q. This indicates that the description of the thermodynamic behaviour for $T \ll T_P$ does not depend too sensitively on the model parameters of the Landau potential in P. The two sets in Table 1 represent two extreme cases, intermediate values would lead to essentially the same temperature evolution of Q and P at temperatures below the melting point.

Finally we have to adress the question of the predicted first order jump near 552 K. A discontinuity has not been reported from experiments, but none of the applied methods had sufficient resolution to completely rule out a discontinuity of the suggested magnitude (Poon, Wruck, Reeder, private communication). Levanyuk et al. (1978) and Salje (1988) give several mechanisms by which phase transitions following a 1st order behaviour may become continuous or rounded due to fluctuations in a small Ginzburg interval near T_{tr}.

The excess free energies of the phase I, II, and III are shown in Fig. 10. Outside the temperature interval indicated by the two vertical lines a free energy can not be assigned to phase III as it no longer corresponds to a minimum in P^2-Q^2 space. The behaviour of P^2 (Fig. 9), in particular for $T<552$ K, resembles the behaviour of a critical fluctuation amplitude peaked at the transition temperature, however, the critical divergence is limited (finite) and spread out in temperature. A qualitatively similar theoretical result for mean square *local* fluctuation amplitudes near phase transitions is discussed by Meissner and Binder (1975) who considered approximations to an integration (Fourier transform) over all collective fluctuation amplitudes in **q** space. As discussed above, however, the ordering phenomenon characterized by P^2 in $NaNO_3$ may be related to spacial inhomogeneities, but it is most probably not related to a classical Ginzburg interval. Figure 11 demonstrates that the model calculation based on classical Landau theory does indeed result in a phenomenological critical exponent close to 0.22 for temperatures between 460 K and 552 K. The temperature bracket of ca. 2 K around T_{tr} where our model seems to fail may indeed represent a genuine Ginzburg interval in which critically divergent fluctuations have to be considered. An explicit consideration of spatial fluctuations may also lead to a rounding of the crossover at 468 K. We also do not exclude the existence of a very small non-zero value of P^2 in the real system below the crossover temperature due to fluctuations.

4.3. Structural Implications and Potts Model Behaviour

So far no direct structural observation of an ordering process corresponding to P has been reported in the literature. In a careful analysis of the electron density of $NaNO_3$ at room temperature, however, Göttlicher and Knöchel (1980) found that the maxima of the probability density of the oxygen positions are in fact very slightly displaced from the diad, with the $R\bar{3}c$ symmetry due to statistical distribution of *pyramidal* NO_3 groups in two equivalent orientations. Zone centre long range correlation of this statistical variable leads to the *R3c* symmetry of the ferroelectric phase observed at pressures exceeding 45 kbars (Barnett et al. 1969). Although this feature is very subtle at room temperature, we cannot exclude that it also leads to a non-zero ordering amplitude at higher temperatures. In fact, Harris and Salje (1989) observed the appearance of a second out-of-plane bending mode of the NO_3 molecule in the temperature range in question. The intensity behaviour of this mode corresponds to the behaviour of P^2, and it may well indicate an ordering process involving non-planarity of the NO_3 group. If P is indeed related to simple crystallographic long range order (rather than a fluctuation process), the assign-

ment of space groups in the various thermal regimes must be reviewed. A further increase in symmetry to a supergroup of $R\bar{3}m$ seems to be incompatible with the structure. Hence, taking $R\bar{3}m$ as the symmetry of phase 0, the space group of phase II should be a subgroup of $R\bar{3}m$. Assuming further that the space group assignment $R\bar{3}c$ for the room temperature phase (I) is correct, the symmetry of phase III must be a common subgroup of $R\bar{3}m$ and $R\bar{3}c$. $R3c$ seems to be an unlikely candidate here, as ferroelectricity is not observed at the relevant pressure conditions. Other possible subgroups of $R\bar{3}m$ should give rise to superlattice Bragg reflections or metric distortions of the lattice, however, none of which have been observed experimentally.

Poon and Salje (1988) and Reeder et al. (1988) discussed the observed sets of phenomenological critical exponents in terms of a classical 'tricritical' Landau behaviour at temperatures $T<460$ K, sufficiently far from the critical temperature, and a fluctuation-dominated regime ($T>460$ K) where the validity of Landau theory breaks down due to the presence of *critical fluctuations* and hence a smaller critical exponent $\beta=0.22$ is observed. The critical exponent α for the excess heat capacity ($c_P \sim T|T-T_c|^{-\alpha}$) is 0.56 (Wruck 1987). Hence the critical exponent γ of the order parameter susceptibility is expected to be close to unity ($\alpha+2\beta+\gamma=2$), which is consistent with the observation that the diffuse intensity near **Z** is inversely proportional to $T-T_c$ (Fig. 3). Poon and Salje (1988) and Reeder et al. (1988) noted the similarity between the observed exponents and those calculated from renormalization-group techniques for a 3-state Potts model (including the effects of a random field) in three dimensions (Burkhardt et al. 1976), i.e. $\alpha=0.55$, $\beta=0.23$ and $\gamma=0.98$. However, three energetically equivalent geometrical configurations dominating the fluctuations of orientational ordering are incompatible with the symmetry of the active irreducible representation $Z_2(A_{1u})$ at the **Z** point.

In our numerical model, these postulated critical fluctuations are essentially replaced by the amplitude P. It can be argued that the set of phenomenological critical exponents obtained is devoid of any physical meaning because the considered temperature range is too large and the phase transition may be slightly of first order as found by our analysis. Nevertheless we will present some arguments based on our results from order parameter coupling in classical Landau theory which indeed can be interpreted in favour of a 3-state model: short range correlations at the point **F** on surface of the Brillouin zone, which locally break the threefold symmetry, have been observed in molecular dynamics simulations by Lynden-Bell et al. (1989). The **F**-point correlations involve rotation – translation coupling, which is symmetry-forbidden at the **Z**-point, but is significantly lowering the energy of domain walls. (We also found a corresponding maximum of diffuse scattering experimentally at the position (1.5, 1.5, 0) predicted by Lynden-Bell et al. (1989); this diffuse scattering intensity, however, is much weaker than that occuring close to the **Z** point.) The fluctuations or diffuse intensity near the **Z** point correspond to long-wavelength modulations of the **Z** point ordering scheme which represents the equilibrium structure of the ordered $R\bar{3}c$ phase. They can be interpreted as due to antiphase boundaries between ordered $R\bar{3}c$ clusters, with the modulation wavelength corresponding to the size of ordered clusters (taking the average, the full width at half maximum of the diffuse peak corresponds to the inverse of the correlation length). The importance of these ordered clusters is highlighted in the observation, that optic phonons which are Raman active in the ordered $R\bar{3}c$ phase, but non-raman active for $R\bar{3}m$ symmetry, still have 50% of their room temperature intensity well above the transition temperature (Poon and Salje 1989). It is most likely that the **F**-point correlations are connected to a local ordering scheme and/or displacement pattern occuring at the interfaces between **Z**-clusters in the sense of an interphase of a wetting phenomenon and correspond to the second ordering amplitude P (Fig. 12). Such phenomena have been studied in great detail by Monte Carlo simulations (Pesch and Selke 1987), where in particular 3-state Potts models have been used. Between two blocks of bulk materials of pseudo spin $+1$ and -1, respectively, an interphase of pseudo spin 0 occurs. The size of the interphase regions usually has its maximum close to the transition temperature of the bulk material. As a common feature of all models producing similar structures, the free energy of the two bulk phases and the interphase is approximately (or exactly) degenerate. Figure 10 shows that the phase III occurs in a temperature range were the excess free energies of ordered clusters (curve I) and the excess free energy of the interphase regions (curve II) are approximately degenerate. As the degeneracy is lifted at temperatures sufficiently far from $T_{tr}=552$ K, the interphase regions (P) disappear. Thus the three structural states in question may be represented by the *i)* 'positive' and *ii)* the 'negative' possibilities of **Z**-point ordering, and *iii)* the interphase structure.

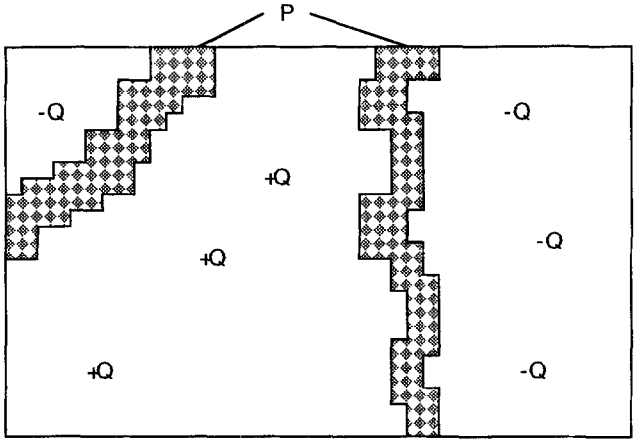

Fig. 12. Schematic illustration of the suggested interface structure between antiphase domains of **Z**-point long range order

Finally it becomes clear why the order parameter P can not represent crystallographic long range order and has not yet been unambiguously identified in experiments: the structure corresponding to P can only occur at **Z** structure interfaces (domain boundaries) and thus the volume fraction of P structure is very limited. As there is no long-range correlation between these interfaces, and positive and negative gradients of **Z** order may appear with equal probability, the spatial average of P is zero and only its mean square amplitude is of thermodynamic importance.

Acknowledgements. It is a pleasure to thank Drs. M.T. Dove, R.M. Lynden-Bell, W.C.K. Poon, R. Reeder and in particular B. Wruck for fruitful discussions and communication of results prior to publication. Prof. P.J. Herley kindly provided the sample of $NaNO_3$ for this study. WWS was supported by NATO stipendium 300/009/501/8 via the Deutscher Akademischer Austauschdienst, Bonn.

References

Barnett JD, Pack J, Hall T (1969) Structure determination of a ferroelectric phase of sodium nitrate above 45 kbar. Trans Am Cryst Assoc 5:113–131

Brehat F, Wyncke B (1985) Analysis of the temperature dependent infrared active lattice modes in the ordered phase of sodium nitrate. J Phys C: Solid State Phys 18:4247–4259

Brown GE, Sueno S, Prewitt CT (1973) A new single-crystal heater for the precession camera and four circle diffractometer. Am Mineral 58:698–704

Bruce AP, Cowley RM (1981) Structural phase transitions. Taylor & Francis, London

Burkhardt TW, Knops HJF, Nijs M (1976) Renormalization-group results for the three-state Potts model. J Phys A 9:L179–181

D'Alessio GJ, Scott TA (1971) Pressure and temperature dependence of the nuclear quadrupole coupling constant of ^{23}Na in single crystal sodium nitrate. J Magn Reson 5:416–428

Dove MT, Powell BM (1989) Neutron diffraction study of the tricritical orientational order/disorder phase transition in calcite at 1260 K. Phys Chem Minerals 16:503–507

Ginzburg VL, Levanyuk AP, Sobyanin AA (1987) Comments on the region of applicability of the Landau theory for structural phase transitions. Ferroelectrics 73:171–182

Göttlicher S, Knöchel CD (1980) Die Elektronendichteverteilung in Natriumnitrat ($NaNO_3$). Acta Crystallogr B36:1271–1277

Gufan YuM, Larin ES (1980) Theory of phase transitions described by two order parameters. Sov Phys Solid State 22:270–275

Harris M, Salje E (1989) An infrared spectroscopic study of the internal modes of sodium nitrate: implications for the orientational order-disorder phase transition. J Phys. Condensed Matter (in preparation)

Kracek FC (1931) Gradual transition in sodium nitrate. I. Physicochemical criteria of the transition. J Am Chem Soc 53:2609–2624

Kracek FC, Posnjak E, Hendricks SB (1931) Gradual transition in sodium nitrate. II. The structure at various temperatures and its bearing on molecular rotation. J Am Chem Soc 53:3339–3348

Lefebvre J, Currat R, Fouret R, More M (1980) Etude par diffusion neutronique des vibrations de reseau dans le nitrate de sodium. J Phys C: Solid State Phys 13:4449–4461

Lefebvre J, Fouret R, Zeyen ME (1984) Structure determination of sodium nitrate near the order-disorder phase transition. J Phys (Paris) 45:1317–1327

Levanyuk AP, Osipov VV, Sigov AS, Sobyanin AA (1980) Change of defect structure and the resultant anomalies in the properties of substances near phase transition points. Sov Phys JETP 49:176–188

Lynden-Bell RM, Ferrario M, McDonald IR, Salje E (1989) A molecular dynamics study of orientational disorder in crystalline sodium nitrate. J Phys Condensed Matter 2 (in press)

Meissner G, Binder K (1975) Debye-Waller factor, compressibility sum rule, and central peak at structural phase transitions. Phys Rev B 12:3948–3955

Neumann G, Vogt H (1978) Rayleigh wing scattering in disordered sodium nitrate. Phys Status Solidi b85:179–184

Paul GL, Pryor AW (1972) The study of sodium nitrate by neutron diffraction. Acta Crystallogr B28:2700–2702

Pesch W, Selke W (1987) Depinning and wetting in two-dimensional Potts and chiral clock models. Z Phys B – Condensed Matter 69:295–301

Petzelt J, Dvorak (1976) Changes of infrared and Raman spectra induced by structural phase transitions: II. Examples. J Phys C: Solid State Phys 9:1587–1601

Poon WCK, Salje E (1988) Excess optical birefringence and phase transition in sodium nitrate. J Phys C: Solid State Phys 21:715–729

Poon WCK, Salje E (1989) Raman spectroscopic investigation of the phase transition in $NaNO_3$. (in preparation)

Reinsborough VC, Wetmore FEW (1957) Specific heat of sodium nitrate and silver nitrate by medium high temperature adiabatic calorimetry. Aust J Chem 20:1–8

Redfern SAT, Salje E, Navrotsky A (1989) High-temperature enthalpy at the orientational order-disorder transition in calcite: implications for the calcite/aragonite phase equilibrium. Contrib Mineral Petrol 101:479–484

Reeder RJ, Redfern SAT, Salje E (1988) Spontaneous strain at the structural phase transition in $NaNO_3$. Phys Chem Minerals 15:605–611

Salje E, Viswanathan K (1976) The phase diagram calcite – aragonite as derived from crystallographic properties. Contrib Mineral Petrol 55:55–68

Salje E, Devarajan V (1986) Phase transitions in systems with strain induced coupling between two order parameters. Phase Trans 6:235–248

Salje E (1988) Structural phase transitions and specific heat anomalies. In: Salje E (ed) Physical properties and thermodynamic behaviour of minerals. NATO ASI series C, vol 255, pp 75–114

Schmahl WW (1988) Diffraction intensities as thermodynamic parameters: orientational ordering in $NaNO_3$. Z Kristallogr 182:231–233

Shen TY, Mitra SS, Prask H, Trevino SF (1975) Order-disorder phenomenon in sodium nitrate studied by low frequency Raman scattering. Phys Rev B 12:4530–4533

Strømme KO (1969) The crystal structure of sodium nitrate in the high-temperature phase. Acta Chem Scand 23:1616–1624

Terauchi H, Yamada Y (1972) X-ray study of phase transition in $NaNO_3$. J Phys Soc Jpn 33:446–454

Wruck B (1987) Unpublished data

Yasaka H, Sakai A, Yagi T (1985) A central peak in the order-disorder phase transition of sodium nitrate. J Phys Soc Jpn 54:3697–3700

Received March 8, 1989